# Structural assessment of concrete beams strengthened with CFRP laminate strips by their dynamic response

## Avaliação estrutural de vigas de betão armado reforçadas com lâminas CFRP por sua resposta dinâmica

Rolando Salgado
A. Gustavo Ayala
José G. Rangel


## Abstract

This paper addresses the location and detection of damage on concrete beams strengthened with CFRP laminates through their dynamic response. For this purpose, three beams with different CFRP strengthening were tested to failure with ambient vibration tests, AVTs, performed before and after damage. Several vibration based damage detection methods were applied to the modal parameters and acceleration histories acquired on the beams evaluating their effectiveness to locate and detect damage with a limited number of measuring points. Finite element models of the beams with properties calibrated with the modal parameters determined from the AVTs were used for calculating their dynamic responses and evaluating the damage detection methods. Results showed that dynamic behaviour of strengthened beams with CFRP laminates does not change significantly compared with no strengthened beam. Moreover, damage was detected when was chosen a denser number of measuring points from the finite element models for all evaluated methods.

## Resumo

Este trabalho aborda a localização e deteção de danos em vigas de betão armado reforçadas com lâminas de CFRP através de sua resposta dinâmica. Para este fim, foram testadas três vigas com reforço de CFRP diferente, com ensaios de vibração ambiental realizados antes e após o dano. Vários métodos de deteção de danos baseados em vibrações foram aplicados aos parâmetros modais e acelerações adquiridos nas vigas avaliando a sua eficácia para localizar e detetar danos com um número limitado de pontos de medição. Modelos de elementos finitos das vigas com propriedades calibradas com os parâmetros modais determinados a partir dos ensaios de vibração ambiental foram utilizados para calcular as suas respostas dinâmicas e avaliar os métodos de deteção de dano. Os resultados mostraram que o comportamento dinâmico de vigas reforçadas com lâminas de CFRP não se altera significativamente em comparação com vigas sem reforço. Além disso, os danos foram detetados quando foi escolhido um número mais denso de pontos de medição a partir dos modelos de elementos finitos para todos os métodos avaliados.


Keywords: CFRP laminates / Concrete beams / Damage detection / Dynamic behaviour / Structural assessment

Palavras-chave:

**Rolando Salgado**

PhD, Assistant Professor
Universidad Veracruzana, Campus Veracruz
Boca de Río, Veracruz, Mexico
rosalgado@uv.mx

**A. Gustavo Ayala**

PhD, Research Professor
Institute of Engineering, UNAM
Mexico City, Mexico
GAyalaM@iingen.unam.mx

**José G. Rangel**

PhD, Assistant Professor
Universidad Veracruzana, Campus Córdoba-Orizaba
Cd. Mendoza, Veracruz, Mexico
gurangel@uv.mx



SALGADO, R. [*et al.*] – Structural assessment of concrete beams strengthened with CFRP laminate strips by their dynamic response. **Revista Portuguesa de Engenharia de Estruturas**. Ed. LNEC. Série III. n.º 4. ISSN 2183-8488. (julho 2017) 37-46.

## 1 Introduction

Composite Fibre Reinforced Polyester (CFRP) has become an important material for strengthening structures. The advantages of this material are, among others, its low weight, ease of installation, high durability and large deformation capacity. However, it has disadvantages such as the fact of its structural performance may be affected by freeze/thaw cycles and its vulnerability against vandalism acts. To minimize and even eliminate these disadvantages, these CFRP laminates are placed into grooves made on the concrete cover of the element to be strengthened. The increment of the structural capacity of reinforced concrete elements strengthened with this material has been reported in several works (*e.g.*, [1], [2] and [3]). However, these studies have been focused in the static behaviour of the strengthened structures and no investigation has been carried out on the change of the dynamic behaviour of reinforced concrete beams strengthened with composite laminates into slits.

It is a widely recognized fact that the dynamic characteristics of an otherwise undamaged structure change when damage is present. This fact has motivated the scientific community to perform dynamic tests on structures such as buildings and bridges. Unfortunately, for damage evaluation purposes, the dynamic parameters for the baseline condition of these structures are required, information that for most cases is not easily available. Available literature shows results of a limited number of dynamic tests performed in real structures before and after deliberate damage is produced ([4] and [5]). Alternatively, simple structures like beams have been investigated to obtain their dynamic responses before and after damage is deliberatively induced. In this way, Maeck ([6]) carried out several tests on concrete beams tested to the failure to validate the direct stiffness calculation method. Cao *et al.* ([7]) used complex wavelet curvature to reduce noise and detect damage in cracked specimens with different boundary conditions. Other experiments carry out in reinforced concrete elements and a review of the most important vibration based damage detection methods can be consulted in [8].

The objective of this paper is to investigate the dynamic behaviour of reinforced concrete beams strengthened with composite laminates and the potential of existent damage detection methods to detect and locate, through the vibration data analysis, damage introduced to these concrete beams. To validate the experimental data found, a numerical Finite Element Model (FEM) of the reinforced concrete beams strengthened with composite laminates will be used. The properties of this model will be updated using the experimental modal parameters. Damage was simulated by modifying the Young's modulus along the length of the beams.

## 2 Main structural characteristics of beams

To accomplish the objectives described above, a series of laboratory tests were carried out on three reinforced concrete beams strengthened with composite laminates. These tests were also part of a series of static tests performed on these specimens aimed to the evaluation of the increment of ductility due to CFRP laminates strengthening ([9]). The three beams used in this study were built with the same steel reinforcement with a nominal yield strength of 415 MPa. All the beams were casted at the same time and compressive strength of the concrete, *f'c*, at 28 days was 40.07 MPa. At the time that the tests on the beams were carried out, the mean compressive resistance of the concrete for the three beams was 44.38 MPa with a standard deviation of 1.06 MPa. One of these beams (referred as CI), used as reference, was built without strengthening. In the other two beams (referred as CII and CIII), composite laminates were placed on their upper surface. All beams were 5.85 m long and had a rectangular cross section of 0.120 m depth and 0.375 m wide. The beams were supported at three points. One support was located at the middle of the beam and the remaining two near the ends of the beams. Small cantilevers, 0.125 m long were considered at the ends of the beams. It resulted to two equal spans with 2.8 m. The end supports were only restricted in the vertical direction while the middle support was clamped. In the first strengthened beam, CII, three CFRP laminate strips were placed at the middle span of the beam. For the other strengthened beam, CIII, the number CFRP laminate strips was increased to 7, all located at the same position as those of the CII beam. The three beams were tested to failure applying a monotonic load in two different locations along their length. Same magnitude loads were simultaneously applied at the middle of the beam spans. These applied forces were distributed across the upper face through metallic plates. The geometrical properties of the beam, the location and quantity of their reinforcement steel and the locations of the strengthening and the applied forces are shown in Figure 1.

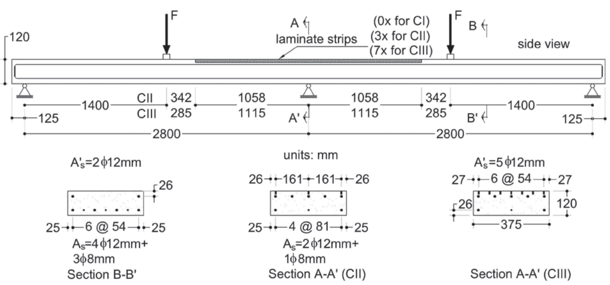


Figure 1 Geometrical properties of the beams

## 3 Failure tests

The failure of the reference beam (CI) was reached when the load at each application point was 52.88 kN. At these points, the maximum residual displacements, after loading was removed, were 53 mm. The failure of the CI beam was characterized by yielding of the steel reinforcement and crushing of the concrete. For the strengthened beam CII, the failure was reached when the load at each application point was 58.78 kN, *i.e.*, an 11.15% increment with respect to the corresponding reference beam, CI. The maximum permanent displacements after failure at the points of load application were 69.5 mm. The failure for the CII beam was due to shear. The failure of beam CIII was reached when the load at each application point was 63.62 kN. For this beam the maximum load increased 20.30% with respect to the reference beam, CI. The permanent displacement at the points of load application after failure was 40.3 mm. A bending failure characterized by rupture of the CFRP laminate strips, yielding of the reinforced steel and concrete crushing occurred in the beam. Additional details regarding the failure mode and the strength increment of the beams with CFRP laminates can be consulted in [9]. The instrumentation layout and the deflection attained of a beam after test are illustrated in Figures 2a and b.

a) Layout instrumentation, static test

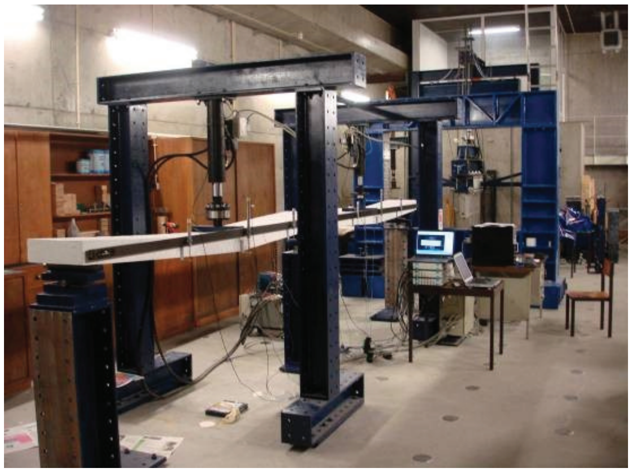

b) Beam deflexion after failure test

Figure 2 Example of the failure test procedure

## 4 Experimental dynamic tests

Dynamic tests were performed on three beams before and after damage. Eight piezoelectric accelerometers (model PCB 393B12) with a nominal sensitivity of 1000 mV/g and an impact hammer (model PCB 086D20), instrumented with a load cell with a nominal sensitivity of 0.24 mV/N, were connected to a DAQ System (cDAQ National Instruments) with two vibration input modules (National Instruments 9134) of four channels each one, able to simultaneously acquire at rates up to 51.2 kS/s. All these sensors deviate of their nominal sensitivity value according to the calibration performed by

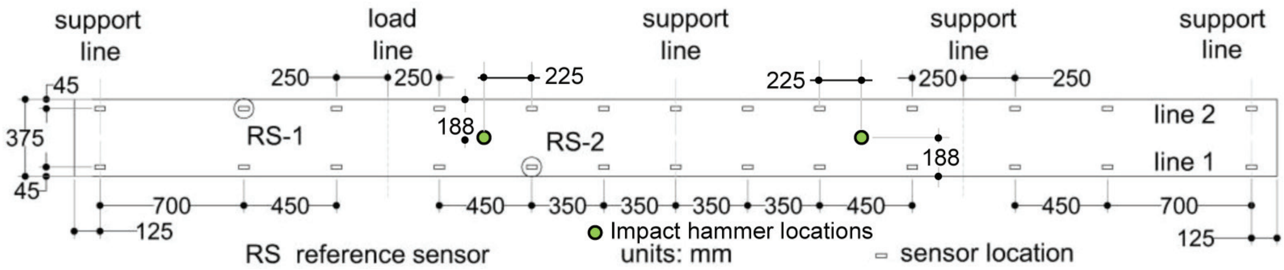


Figure 3 Position of sensors for the dynamic tests

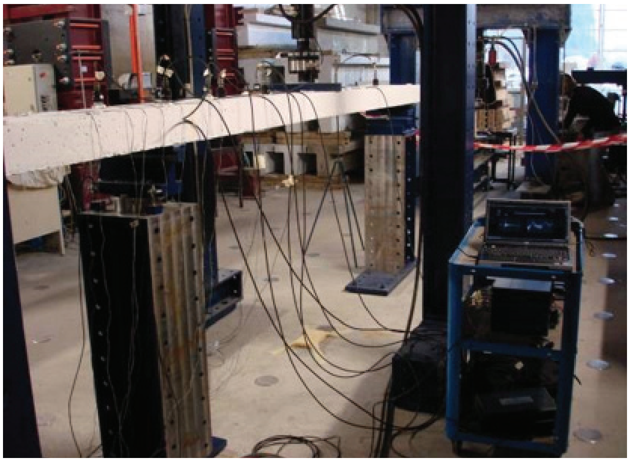

a) Ambient vibration tests, AVTs

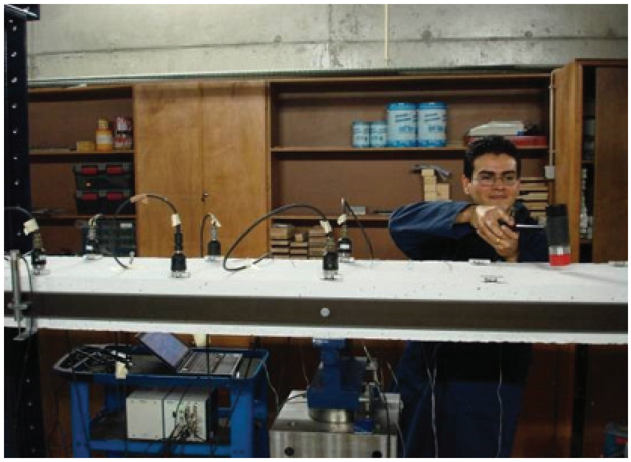

b) Impact hammer tests, IHTs

Figure 4 Example of the dynamic test procedures

the manufacturer. The sensitivity values of each sensor were taken into account during dynamic tests. During the dynamic tests only the responses of the vertical DOFs were registered. Two reference sensors were kept at fixed position and the remaining six were moved four times for covering all the nodes along the beams' models used for the analyses. The acceleration time histories of the AVTs were recorded during 150 s (according to the recommendation given by [10]) with a sampling rate of 600 Hz. Besides the AVTs, the beams were subjected to Impact Hammer Tests (IHTs). The beam specimen was excited with a single hammer impact in two locations as shown in Figure 3. To have a good waveform definition, the acceleration response caused by this hammer impact was recorded during 10 s with a sampling rate of 7500 Hz. The IHTs were used to determine the damping ratios of the beams using the logarithmic decrement method (LDM) ([11]) and the area method (AM) ([12]). Because IHTs have a great variability, several IHTs were performed for each location selecting that with the best waveform quality. Data acquired from the IHTs was not used to determine other modal parameters because beams were excited just in two locations by an impact force. In this context AVTs are more precise because the beams are excited in all points with different intensities. The locations of the accelerometers with the impact hammer and an example of the dynamic test procedures are depicted in Figures 3 and 4, respectively.

## 5 Modal analysis

From the recorded acceleration time history, modal identifications of the beam specimens were carried out using the enhanced frequency domain decomposition method ([11]). To do that, the acceleration time history, acquired at 600 Hz without decimation, was filtered using a bandpass Butterworth filter at 5 and 250 Hz with a slope of 48 dB/octave. Spectral density matrices were estimated performing a Fourier Transform of the acquired data, broken in segments of 1024 elements, and multiplied by the Hanning window function. Finally, this data was averaged with a 67% overlap. In total, six modal parameters were identified. Three of them were done on the undamaged specimens (CI, CII and CIII) and the remaining three were done on the same specimens after damage (cases DI, DII and DIII). The dynamic parameters of the beams were calculated using a program developed in Matlab ([13]). Five resonant natural frequencies and their corresponding mode shapes were identified for each case. As an example, the modal parameters for the cases CII and DII are given in Figures 5a to 5e and Figures 5f to 5j, respectively.

The first two mode shapes for all cases studied corresponded to the first and second vertical bending modes and the third shape to a torsional mode. As mentioned before, beam rotations at its intermediate support were not allowed, *i.e.*, the beam was clamped. However, as this support was fixed to a column just with a screw, something that might had allowed displacements, small enough to permit a torsional mode shape to be developed. The third and fourth mode shapes corresponded to the third vertical bending mode and the second rotational mode. These modes exchanged their relative positions after damage, *i.e.*, 4th mode before damage became 5th mode after damage and 5th mode before damage became 4th mode after damage.

The procedure for the IHTs consisted in determining the power spectral density function of the free vibration response for each measuring point at each of the hit positions indicated in Figure 3. This power spectral density function was then filtered to eliminate the information outside the frequency of interest. In a next step, the inverse discrete Fourier transform of the filtered power spectral density was obtained (also called autocorrelation function). From the autocorrelation function, the maximum extreme values (for the LDM) and the time at which the autocorrelation function crossed zero were determined (for the AM). Finally, the damping ratio was calculated either as the slope of the curve of the logarithm of the absolute extreme values (for the LDM) *versus* the time lag, or the logarithm of the area covered within two consecutive times that the function crossed zero (for the AM), *versus* the same time lag. The procedure followed for calculating the damping ratio with the above described methods is illustrated in Figure 6.

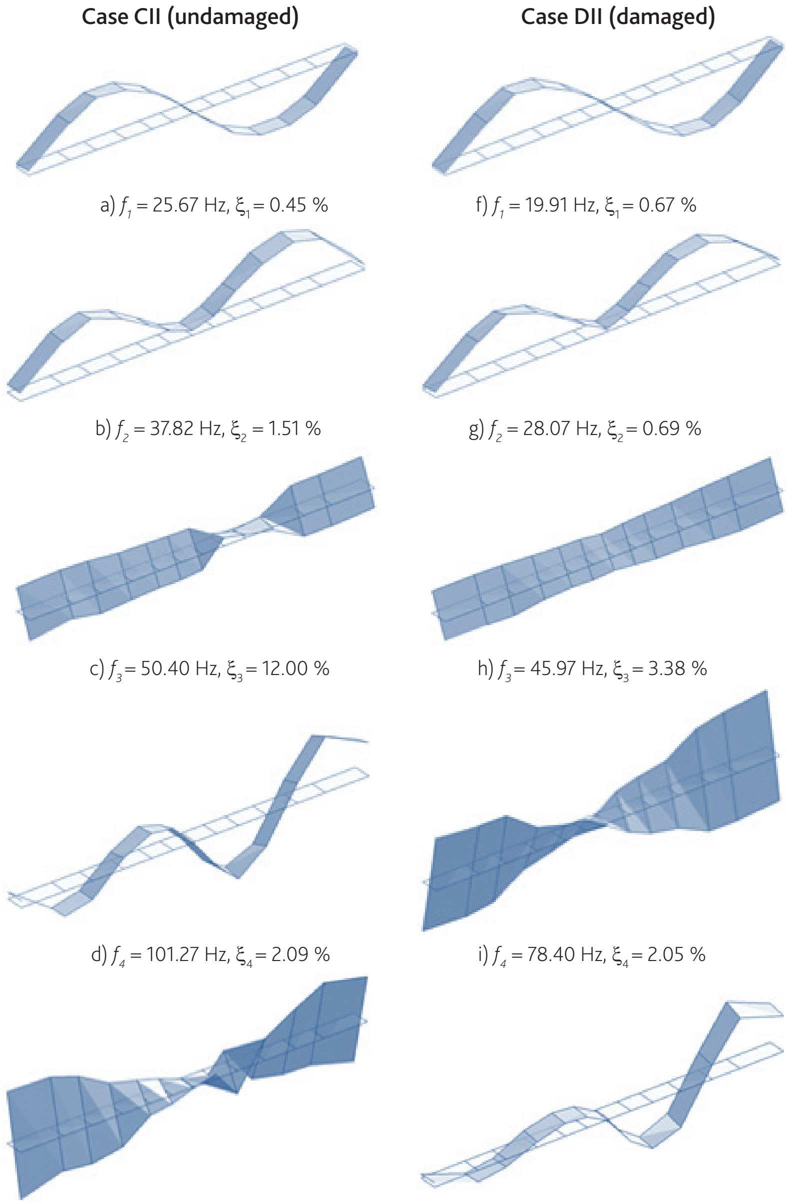


a) $f_1$ = 25.67 Hz, $\xi_1$ = 0.45 %

f) $f_1$ = 19.91 Hz, $\xi_1$ = 0.67 %

b) $f_2$ = 37.82 Hz, $\xi_2$ = 1.51 %

g) $f_2$ = 28.07 Hz, $\xi_2$ = 0.69 %

c) $f_3$ = 50.40 Hz, $\xi_3$ = 12.00 %

h) $f_3$ = 45.97 Hz, $\xi_3$ = 3.38 %

d) $f_4$ = 101.27 Hz, $\xi_4$ = 2.09 %

i) $f_4$ = 78.40 Hz, $\xi_4$ = 2.05 %

e) $f_5$ = 116.80 Hz, $\xi_5$ = 1.48 %

j) $f_5$ = 92.42 Hz, $\xi_5$ = 1.97 %

**Figure 5** Determined mode shapes, CII and DII cases

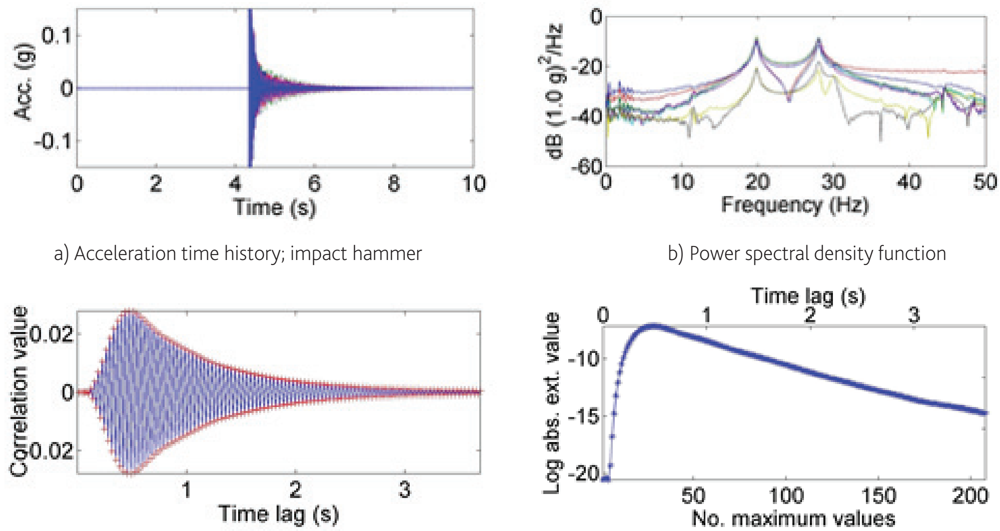


a) Acceleration time history; impact hammer

b) Power spectral density function

c) Autocorrelation for the 1st frequency

d) Logarithmic envelop

Figure 6 Procedure followed for calculating the damping ratios using data from IHTs

## 6 Finite element model of the beam specimens

Initial Finite Element Models (FEMs) of the beams before and after damage were carried out in the structural analysis program SAP2000 ([14]). The models consisted of 648 nodes each with 6 DOFs, the concrete beams were modelled with 544 thick shell elements 120 mm deep, 24 frame elements for the steel bars with a diameter of 7.5 mm. For the properties of the concrete, relevant data for obtaining the numerical modal parameters of the beams, a Young's modulus of 35.55 GPa was determined according to Eurocode 2 ([15]), a compressive strength of 44.38 MPa and a mass density of 2.4 ton/m$^3$ were obtained. The Young's modulus of the CFRP laminates, 200 GPa, was not included in the models as its influence in the dynamic behaviour of the beams was not significant and did not justify a more complex FEM. Instead of that, small deviation of the Young's modulus from its mean value took the small differences in the modal parameters between the undamaged specimens. The natural frequencies and mode shapes of the FEMs were obtained using the Ritz Vector procedure. The end supports of the beams were restrained in their transversal and vertical displacements, $u_2$ and $u_3$, and in their rotation $r_3$ around the vertical direction. In the middle support, the beams were clamped allowing only small rotations about $r_1$. The FEM of the beams is shown in Figure 7.

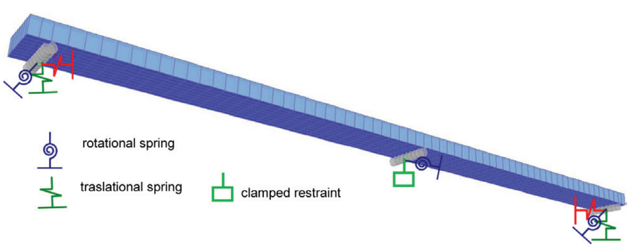


Figure 7 FEM of the beams

## 7 Model updating

The initial FEMs of the undamaged beams (CI, CII and CIII) were updated by tuning its physical properties and boundary conditions to match its natural frequencies and mode shapes with those determined from the AVTs. Only the first two natural frequencies of the undamaged beams were taken into account in the model updating process. In fact, these parameters were determined, with the highest accuracy in the experimental tests. For instance, the coefficients of variation (COV) for the first two frequencies were less than 1% in all cases evaluated, while for some of the remaining Eigen frequencies the COVs were more than 1% (see [16] for more details about modal parameters and their COV).

For the FEMs of the beams, three parameters were considered to have an important influence in their dynamic behaviour, *i.e.*, the average Young's modulus of the concrete $E$ and the vertical translation $u_3$ at the supports of the beams. Using the FEM models a sensitivity analysis was carried out to determine the sensitivity coefficients of the natural frequencies, $f_i$, to the selected parameters, $Pr_j$. For this, a common method for calculating these sensitivity coefficients in structural engineering ([17]) was used. These coefficients are obtained using the following equation:

$$S_{i,j} = f_i^{-1}\left[\frac{\partial f_i}{\partial Pr_j}\right] Pr_j \qquad (1)$$

where $S_{i,j}$ is the normalized sensitivity matrix and subscripts $i = 1$, ...$N$ for $N$ frequencies and $j = 1$, ...$M$ for $M$ parameters. For the case study $M = 3$ parameters, namely: Young's modulus and vertical translations at end and middle supports. $N = 2$ frequencies. Using these values, the best matchings of results with the experimental tests were obtained.

The sensitivity coefficients given in Table I showed that the Young's modulus, $E$, had an important influence in the natural frequencies. The vertical translations $u_3$ at the end supports and at the middle of the beam also had influence in the frequencies but in less measure. Therefore, the Young's modulus and the vertical translation parameters were considered as the sensitive parameters for the model updating process.

Table I Sensitivity coefficients in percentage

| Frequency | $E$ | $u_3$ middle | $u_3$ end |
|---|---|---|---|
| 1 | -109.27 | 0.00 | -3.09 |
| 2 | -64.92 | -14.58 | -2.80 |

A manual model updating process was done tuning the three sensitive parameters in the FEM of the undamaged beams. This procedure was repeated until a predefined level of accuracy was achieved in the differences between the experimental and numerical natural frequencies and mode shapes. The final correlation determined for the three undamaged specimens is given in Table II.

The final values of the sensitivity parameters given in Table II indicate that the Young's modulus suffered variations less than 4% of the value adopted for the initial FEM. The vertical translation $u_3$ of the middle support required significant changes from its initial value to match the second mode shape and corresponding natural frequency.

Table II Final value of the sensitivity parameters after the model updating process (undamaged cases

| Parameter | Initial model | CI | CII | CIII |
|---|---|---|---|---|
| $E$ (GPa) | 35.55 | 36.95 | 36.18 | 36.39 |
| $u_3$ middle (kN/m) | 100000 | 112000 | 90500 | 78000 |
| $u_3$ end (kN/m) | 100000 | 95500 | 95500 | 95500 |

## 8 Dynamic simulation of damaged beams

The dynamic behaviour of the damaged beams was determined simulating the structural damage into the updated FEMs of the undamaged beams. Damage was simulated with a modification of the flexibility of the beam at the damage zones using the Modified Christides and Barr method ([16]). Considering that at the damage zones the moments of inertia $I$ of the cross sections of the beams remained constant, their Young's modulus varied according to Equation 2:

$$E(x)=\frac{E_0}{1+C_{cr}\,exp(-2\alpha_{cr}\,|x-x_j\,|/h)} \quad (2)$$

where $x$ defines the location of the point to the left of the support where the Young's modulus is calculated, $x_j$ defines the crack positions, $E_0$ is the Young's modulus of the beam for the undamaged specimen, $C_{cr}=(I-I_{cj})/I_{cj}$, $I$ is the moment of inertia of the undamaged beam section, $I_{cj}$ is the moment of inertia of the damaged section at the location of the $j_{th}$ crack, $h$ is the depth of the undamaged beam and $\alpha_{cr}$ is an experimentally defined coefficient whose value was set to 2.267.

The variation of the Young's modulus along the beam is shown in Figure 8 where darker blue colours indicate Young's modulus nearing those determined for the undamaged specimens given in Table I. On the other hand, lighter blue colours indicate Young's modulus nearing zero value.

A manual model updating process was done tuning the three sensitive parameters in the FEM of the undamaged beams. This procedure was repeated until a predefined level of accuracy was achieved in the differences between the experimental and numerical natural frequencies and mode shapes. The damage patterns of the beams in the three damage zones included cracks different in size, direction and depth. In the FEMs equivalent single vertical open cracks at the damaged positions were instead considered. The depth of these equivalent vertical cracks was determined matching the numerical modal parameters of the damaged beams with their experimental ones. The final correlation determined from this manual model updating procedure is given in Table III.

Figure 8 Variation of the Young's modulus along the damaged beams (– – support line)

Table III Correlation between the numerical and experimental modal parameters of damaged specimens

| Parameter | Case DI | | Case DII | | Case DIII | |
|---|---|---|---|---|---|---|
| | mode 1 | mode 2 | mode 1 | mode 2 | mode 1 | mode 2 |
| $f_e$ (Hz) | 20.04 | 28.78 | 19.91 | 28.07 | 20.62 | 26.78 |
| $f_n$ (Hz) | 20.47 | 28.27 | 20.16 | 27.65 | 20.15 | 27.48 |
| $\Delta f$ (%) | -2.08 | 1.82 | -1.23 | 1.51 | 2.33 | -2.53 |
| MAC | 1.00 | 0.99 | 1.00 | 0.99 | 0.99 | 0.99 |
| NMD (%) | 4.94 | 7.74 | 4.34 | 8.57 | 7.40 | 8.47 |

where $f_e$ and $f_n$ are the frequency obtained from the AVTs simulations and numerical simulations, respectively.

Correlation between natural frequencies gave values below 2.53% larger than the maximum value determined for the undamaged beams but still indicated a good correlation with natural frequencies. For the correlation between mode shapes, the Modal Normalized Difference (NMD) was used. NMD is considered a variant of the Modal Assurance Criterion (MAC) method. The MAC method determines the projection of one vector onto another in such way that both vectors are the same when MAC achieved a value equal to one while a MAC value close to zero indicates that both vectors are uncorrelated. The NMD method is related to MAC method as follows ([16]):

$$NMD\,(\phi_i\phi_i^*)=\sqrt{\frac{1-MAC\,(\phi_i\phi_i^*)}{MAC\,(\phi_i\phi_i^*)}} \quad (3)$$

where $\phi_i$ and $\phi*_i$ are the $i_{th}$ mode shape for the undamaged and damaged conditions, respectively. MAC method is defined as ([16]):

$$MAC\ (\phi_i \phi_i^*) = \frac{|\phi_i^T \phi_i^*|}{(\phi_i^T \phi_i)(\phi_i^{*T} \phi_i^*)} \tag{4}$$

Differences in natural frequencies close to zero and MAC values close to one (equivalent to NMD values less than 12%) are indications of high correlation between the experimental and numerical modal parameters. This characteristic indicates that the FEMs give an accurate representation of the dynamic behaviour of the undamaged beams.

From Table III the NMD gave values below 9.0%, smaller than the maximum values determined for the undamaged beams indicating an excellent correlation between mode shapes. Therefore, the FEMs of the damaged beams were accurate representations of their prototypes.

The depths of the equivalent vertical cracks ($a_{eq}$) did not show a big variation between the undamaged cases. They increased slightly from the damage case DI with 78.0 mm to 78.6 mm for the damage case DIII. This reflected a similar dynamic behaviour for the first two modes of the damaged cases. The depths of the equivalent cracks and Young's modulus values considered for the damaged cases are given in Table IV.

Table IV Young's modulus and equivalent crack depth values for the damaged specimens

| Parameter | DI | DII | DIII | Colour |
|---|---|---|---|---|
| $a_{eq}$ (mm) | 78.0 | 78.4 | 78.6 | ----- |
| $E_0$ (GPa) | 36.95 | 36.18 | 36.39 | |
| $E_1$ (GPa) | 33.91 | 33.13 | 33.27 | |
| $E_2$ (GPa) | 26.13 | 25.41 | 25.44 | |
| $E_3$ (GPa) | 13.66 | 13.18 | 13.13 | |
| $E_4$ (GPa) | 4.29 | 4.11 | 4.07 | |

## 9 Damage location from simulated dynamic behaviour

For the location of damage in the beam specimens, eight vibration based damage detection methods were used. Four of these methods were based on Wavelet Analysis, *i.e.*, the Continuous Wavelet Transform (CWT), the Discrete Wavelet Analysis (DWA), the Wavelet Packet Signature and the Damage Index applied to the CWT of the mode shapes (CWT-DI). The curvature method, the Damage Index (DI), the change of stiffness and the flexibility methods complement the methods used. The CWT, the DWA and the Curvature methods located damage along the structures only with the vibration parameters determined from the damaged cases. The WPS is the only method that uses the acceleration response for locating the damage. It calculates the energy shape related to the Wavelet Packet Decomposition of the acceleration response of the specimens. An explanation of these methods falls out of the scope of this work. However, a comprehensive explanation of the used damage detection methods may be found in [16].

All mode shapes determined from the AVTs were mass normalized. With the purpose of simplifying the damage location process, the mass normalized mode shapes were divided into two longitudinal lines defined along the beams (see Figure 2). Considering that the used damage detection methods have a better performance when more measurement points are used, the normalized mode shapes and the energy shapes were interpolated from the original 13 points to 113 points along the two lines previously defined using spline interpolation. Additionally, mode shape curvatures were calculated using the smoothing procedure proposed by [6].

For the case of Wavelet Analysis methods (DWA, CWT and WPS), the Gauss no. 4 mother wavelet for the CWT method in the scale no. 2 and the Daubechies no. 4 mother wavelet for the DWA method in the detail no. 1 were the chosen variables. In the WPS method, the acceleration response was decomposed to the 9th level using the Daubechies no. 4 as the mother wavelet. In the WPS method, the five functions with the highest entropy energy were chosen for the damage detection procedure.

The updated FEMs of the beams before and after damage were used for determining their dynamic parameters, in particular, mode shapes and acceleration responses with a higher number of DOFs along the beams. In fact, the location and number of sensors on the beams could play an important role for the location of damage using these methods. As previously mentioned, the number of DOFs defined for these AVTs were set according to practical reasons for space instrumentation and available time for performing the tests. Under these conditions, modal parameter identification was successfully done on all AVTs and frequency changes clearly detected damage for all evaluated cases. However, mode shapes and energy shapes determined from the Wavelet decomposition of acceleration responses were not able to determine the locations of damage for all cases considered.

Two longitudinal lines of nodes were defined on the updated FEMs at the same transversal separation as defined for the experimental dynamic tests. The number of measuring points for each line was 65 evenly separated along the updated FEMs. Under these conditions, mode shapes and acceleration response with this new layout were extracted. Acceleration responses were determined applying two concentrated dynamic forces located at the middle of the beam spans. Their magnitudes were defined as random with a uniform distribution and a mean value of 0.1 N. The time histories of accelerations were obtained with a sampling rate of 600 Hz, the same used for the experimental dynamic tests. For the dynamic simulations, the recorded time was shortened to 16.67 s to reduce the computational effort required for calculating the dynamic response from the updated FEMs. With these adopted conditions, a typical acceleration response determined from the updated FEM is shown in Figure 9.

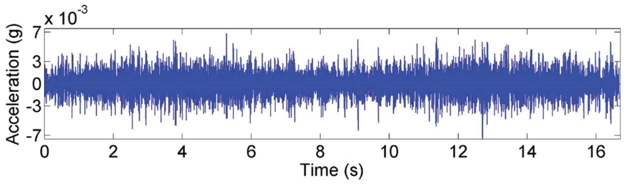


**Figure 9** Acceleration response at the middle of the left span obtained from the updated FEM of the case CI

For the application of the eight damage detection methods, the same conditions defined for the damage location for the experimental dynamic tests were adopted, *i.e.*, type of mother wavelet, level of decomposition of the acceleration response, method for calculating the curvatures of the mode shapes and other required parameters. Spline interpolation between output responses were not done at this step. The number of measuring points was considered enough for an adequate application of the damage detection methods. Typical example of the application of these methods to the simulated dynamic response of the beams determined from the updated FEMs is shown in Figure 10.

The evaluated damage detection methods presented in general give a better performance when compared with their experimental counterparts. All the methods had a disturbance located at the middle of the spans and several of them could also locate damage at the middle support. The CWT-DI method presented the best performance between the selected damage detection methods with coefficient values at the damage zones clearly higher than those outside these areas. Furthermore, this method delimited these disturbances at the damage zones. It seems that combining the characteristics for damage location of CWT and DI methods could increase the probability of damage location. Other damage detection methods performed also well, but their coefficient values at the damage locations and delimited zone of damage were not as good as for the CWT-DI method.

In conclusion, the number of points located in the beams during the dynamic tests was not dense enough for an appropriate damage location. The effects caused by damage in the mode shapes and acceleration responses were concentrated at the close vicinity of the damage zones. Moreover, in this study, the location of damage was known during all the process of damage detection. In the structural evaluation of a real case, location of damage is not known *a priori* and an optimal location of sensors could not be done. Furthermore, to perform dynamic tests in more complex structures like buildings or bridges with a large number of measuring points would not be practical. A better procedure for damage detection would consist of locating some sensors on the probable location of damage and its neighbourhood. At least two different sensor layouts should be considered in this step. Then, update a numerical FEM of the structure with the experimental dynamic parameters. Several patterns of structural damage could be simulated in the structure according the assumed damage locations in the dynamic tests. Next, their influence in the dynamic parameters could be determined. In a subsequent step, the sensor layouts used for the dynamic tests would be upgraded by comparing modal parameters from the simulated damage with experimental ones. If two experimental modal parameter identifications performed on the structure lead

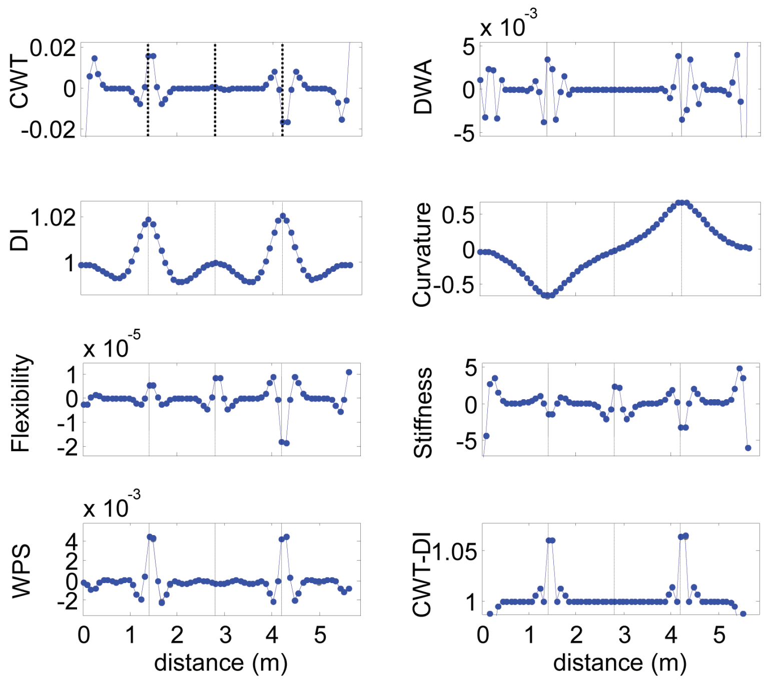


**Figure 10** Typical example of the application of the damage detection methods to the case CII-DII (2nd mode and energy shapes from simulations). Keys —•— line 1 and - - - line 2; damage zone

to significant differences in the evaluated dynamic parameters, the detection and location of damage procedures should be done. Thus, the procedure used here for the damage detection and location on these beams can also be applied to more complex structures using an iterative procedure.

## 10 Conclusions

The modal parameter identification of the three concrete beam specimens showed that the strengthening CFRP laminates added to the beams did not significantly modify their dynamic response even when their ultimate static load, compared with the case without strengthening, increased up to 20.3% for the beam with the highest strengthening. Five mode shapes and their corresponding natural frequencies and damping ratios were identified for each case. Two rotational modes were identified. In the experimental tests, end supports allowed longitudinal rotations and the middle support also allowed small longitudinal rotations.

The dynamic parameters determined from the FEMs were used for locating the damage in the beams through damage detection methods. A denser grid of points was used to compare with the results obtained in the AVTs. The performance of the damage detection methods significantly improved and all methods presented disturbance at the damage zones located at the middle of the spans. The CWT-DI presented the best performance. Combining the advantages of the location features of both methods (CWT and DI) increased the probability of damage location. The results showed in this study highlighted the importance of the sensor layout adopted for the damage detection procedure. The sensor layout does not only need to be larger in quantity compared with the traditional dynamic tests for modal parameter identification, it also requires having more sensors close to the damaged zones. However, damage is not known *a priori* in real scenarios. A FEM of the structure updated with the parameters extracted from the dynamic tests could help firstly to simulate the probable damage scenarios in the structure and secondly to optimize the position of the sensor layout for a better probability of damage location. In summary, the process of damage location with the current development of sensor instrumentation for AVTs and the evaluated vibration-based damage detection methods needs an iterative procedure between experimental dynamic tests and updated FEMs.

## Acknowledgements

The authors would like to thank Professors Everaldo Bonaldo and Joaquim Barros for the opportunity given to perform the dynamic tests on the beams. The first author would also like to thank the Portuguese Foundation of Science and Technology, FCT, for his doctoral grant with reference SFRH/BD/29317/2006.

## References

[1] Guo Y.; Xie J.; Xie Z.; Zhong J. – "Experimental study on compressive behavior of damaged normal and high-strength concrete confined with CFRP laminates". *Construction and Building Materials,* 107, p. 411–425, 2016.

[2] Barros, J. A. O.; Dias, S. J. E.; Lima, J. L. T. – "Efficacy of CFRP-based techniques for the flexural and shear strengthening of concrete beams". *Cement and Concrete Composites,* 29, p. 203-217, 2007.

[3] Gao, P.; Gu, X.; Mosallam, A.S. – "Flexural behavior of preloaded reinforced concrete beams strengthened by prestressed CFRP laminates". *Composite Structures,* 157, p. 33–50, 2016.

[4] Salgado, R.; Cruz, P. J. S. – "Modal identification and damage detection of Övik Bridge between deliberated damage tests – Sustainable Bridges – Assessment for Future Traffic Demands and Longer Lives", internal report, Department of Civil Engineering, University of Minho, Guimarães, Portugal, 2007.

[5] Di Cesare, A.; Ponzo, F. C.; Vona, M.; Dolce, M.; Masi, A.; Gallipoli, M. R.; Mucciarelli, M. – "Identification of the structural model and analysis of the global seismic behaviour of a RC damaged building". *Soil Dynamics and Earthquake Engineering*, 65, p. 131–141, 2014.

[6] Maeck, J. – *Damage assessment of civil engineering structures by vibration monitoring*. PhD dissertation, Catholic University of Leuven. Heverlee, Belgium, 2003.

[7] Cao, M.S.; Xu, W.; Ren, W. X.; Ostachowicz, W.; Sha, G. G.; Pan, L. X. – "A concept of complex-wavelet modal curvature for detecting multiple cracks in beams under noisy conditions". *Mechanical Systems and Signal Processing,* 76-77, p. 555–575, 2016.

[8] Montalvão, D.; Maia, N. M. M.; Ribeiro A. M. R. – "A Review of Vibration-based Structural Health Monitoring with special Emphasis on Composite Materials". *The Shock and Vibration Digest*, 38(4), p. 1-30, 2006.

[9] Bonaldo, E. – *Composite materials and discrete steel fibers for the strengthening of thin structures*, PhD Dissertation, University of Minho, Guimarães, Portugal, 2008.

[10] Cantieni, R. – "Experimental methods used in system identification of civil engineering structures", In Proc. of the 1st International Operational Modal Analysis Conference (IOMAC), Copenhagen, Denmark, p. 249–260, 2005.

[11] Brincker, R.; Ventura, C. E.; Andersen, P. – "Damping estimation by frequency domain decomposition", In Proc. of the 19th International Modal Analysis Conference (IMAC), Kissimmee, FL, USA., 2001.

[12] Huang, F. L.; Wanga, X. M.; Chena, Z. Q.; Hea, X. H.; Ni, Y. Q. – "A new approach to identification of structural damping ratios", *Journal of Sound and Vibration,* 303, p. 144–153, 2007.

[13] MathWorks – *Matlab version 6.5.0.180913a, language engineering computer program*, MathWorks, Inc., Natick, USA, 2002.

[14] CSI – *SAP2000 Advanced 10.0.5. Structural analysis program*. Computers and Structures Inc., Berkeley, CA, USA, 2006.

[15] CEN – *Eurocode 2: Design of concrete structures Part 1: General rules and rules for buildings*, European Committee for Standardization, prEN 1992-1:2001, Brussels, Belgium, 2001.

[16] Salgado, R. – *Damage detection in bridges through vibration monitoring: evaluation and application*, Ph.D. Dissertation, University of Minho, Guimarães, Portugal, 2008.

[17] Brownjohn, J. M. W.; Xia, P. Q.; Hao, H.; Xia, Y. – "Civil structure condition assessment by FE model updating: methodology and case studies", *Finite Elements in Analysis and Design*, 37, p. 761-775, 2001.